Proceedings of the 11th International Conference on Fluid Flow, Heat and Mass Transfer (FFHMT 2024)
Chestnut Conference Centre - University of Toronto, Toronto, Canada – June 16-18, 2024
Paper No. 028
DOI: 10.11159/ffhmt24.028

Terminal Settling Velocity of Cylindrical Rods with Various Geometries Applicable to Atmospheric Microplastics

Amirhossein Hamidi[1], Daniel Daramsing[1], Mark D. Gordon[2], Liisa M. Jantunen[3], Ronald E. Hanson[1]
[1]Department of Mechanical Engineering, York University
4700 Keele St, Toronto, M3J1P0, Ontario, Canada.
Emails: ahamidi7@yorku.ca; danielvd@my.yorku.ca; hansonre@yorku.ca;
[2]Earth and Space Science and Engineering, York University,
4700 Keele St, Toronto, M3J1P0, Ontario, Canada.
Email: mgordon@yorku.ca
[3]Air Quality Processes Research Section, Environment and Climate
Change Canada, 6248 8th Line, Egbert, L0L1N0, Ontario, Canada.
Email: Liisa.Jantunen@ec.gc.ca;

Abstract – In this research, a set of straight, curved, V-shaped, and U-shaped cylindrical rods are dropped in a chamber filled with a quiescent 90% glycerin mixture to approximate the settling of microplastic fibres in the atmosphere. The 3D fall trajectory and terminal velocity of the rods are determined using images captured from two cameras facing the two perpendicular sides of the chamber. The results show that the terminal velocities of the curved and V-shaped rods are both greater than that of the straight rods with the same diameter and aspect ratio, with a maximum difference of 17% and 57% relative to the straight rods for the curved and V-shaped rods respectively within the ranges studied in this research. U-shaped rods always exhibit a greater terminal velocity than straight rods with the same dimensions, with a maximum difference of 39% calculated in this research. As the aspect ratio of a U-shaped rod increases, the terminal velocity initially increases, reaches a peak value, and then decreases, reflecting the interplay between the length of the rod arms and the inclination angle.

***Keywords*:** Microplastics; Microfibres; Settling Velocity; Particle; Environment.

1. Introduction

Microplastics (MPs) are a subset of plastics with sizes ranging between 1 μm and 5 mm [1-3]. MP pollution is known to be spread through the environment, spans the globe from urban to remote areas [4-7], and can pose various risks to human health and ecosystems. For instance, inhaling MPs can lead to respiratory illnesses [8-10]. These particles may also contain harmful components like monomers, chemicals, colors, and additives, which can further endanger human health when inhaled or ingested [11, 12]. Their presence in ecosystems, including food sources like fish and table salt, raises concerns about food safety and potential health issues such as reproductive problems and cancer [13]. The discovery of MPs in Arctic glaciers has ecological implications as they can absorb sunlight, reducing the ice surface albedo. This contributes to accelerated ice melting and disrupts climate patterns [14, 15]. Of reported atmospheric deposition samples, fibres are a prevalent shape, and often the most abundant [2, 5, 16, 17]. Past efforts to model the atmospheric transport of microplastic fibres (MFs) have often relied on simplified representations of shapes such as spheres or a single straight fibre to estimate transport properties such as terminal velocity [6, 18, 19]. In the present research, the settling of rigid cylindrical rods of various finite lengths and shapes are studied to better understand how length and shape can affect microfibre behaviour at the low Reynolds numbers expected in local or global atmospheric transport and to provide input for simulations of atmospheric transport.

Numerous aerodynamic models to estimate the terminal velocity of general non-spherical particles are reviewed by Michaelides and Feng [20]. At the core of modelling predictions is the particle size or shape representation. For example, Ganser [21] modelled the drag coefficient of isometric and nonisometric particles using a generalized Reynolds number, a function of Stoke's and Newton's shape factors, to predict the drag coefficient. In the study conducted by Song et al. [22], drop tests were performed using spheres, cubes, and cylinders of varying sizes and aspect ratios in glycerin mixtures with different viscosities. They introduced sphericity, indicating the ratio of the area of a volume-equivalent sphere to the particle

area, and projected area ratio, indicating the ratio of the projected area of a volume-equivalent sphere to the particle projected area, to model their results. Bagheri and Bonadonna [23] conducted experiments in a vertical wind tunnel to determine the terminal velocity of a wide range of non-spherical particles. They modelled the drag coefficient of irregular particles utilizing the shape factors of flatness (the ratio of shortest length to intermediate length) and elongation (the ratio of intermediate to longest length). Zhang and Choi [24] modelled the terminal velocity of microplastic particles with the ability to differentiate between various shapes, including fibres, films, and fragments. Henn [25] proposed a theoretical correlation for the settling velocity of long cylindrical particles. When comparing the ratio of the aerodynamic equivalent diameter to the fibre diameter (given by D_a/D_C) with the experimental findings, their model exhibits a maximum discrepancy of 6% for glass fibre with a dimeter ranging between 1 and 2 μm and aspect ratios between 5 and 150. Khalili and Liu [26] introduced an approach to estimating the drag coefficient of an infinite cylinder through the numerical analysis of the flow around the cylinder. Huner and Hussey [27] developed a drag coefficient model for an infinite circular cylinder within a Reynolds number range of 0.23 to 2.6, while Sen et al. [28] studied a uniform flow past a cylinder and provided a drag coefficient model applicable for Reynolds numbers between 6 and 40. However, when applied strictly to finite fibres of various shapes, these models all provide significantly varying results, and these results vary with Reynolds number.

The samples from atmospheric deposition reveal that microplastic fibres have a variety of shapes differing from straight [2, 16, 29, 30], highlighting the question of geometry effects on settling behaviour. Rong et al. [31] found that reducing the radius of curvature of a curved fibre increases its terminal velocity and results in a faster achievement of terminal velocity with reduced overshooting. Yang et al. [32] also observed that curved fibres settle faster in their experiments. Nguyen et al. [33] found that larger curliness in fibre geometry leads to a lower terminal velocity, especially for fibres longer than 1 mm. Marchetti et al. [34] investigated the deformation of elastic fibres as they reach their terminal velocity using the dimensionless elasto-gravitational number (β). Their findings indicate that smaller fibres with $\beta < 1000$ adopt a V shape, while larger fibres with $\beta > 1000$ take on a U-shaped geometry. The presence of asymmetry in the geometry or mass distribution of a cylindrical particle can also affect its orientation and terminal velocity. Roy et al. [35] demonstrated that fibres with an asymmetric distribution of radius or mass density experience a transition from a vertical to an oblique orientation as the Archimedes number increases or the degree of asymmetry decreases. A dumbbell-shaped particle made of two spheres connected by a weightless rod, studied by Candelier et al. [39], settles vertically when the two spheres vary significantly in size with the larger sphere at a lower position. However, as the size difference reduces, the orientation changes to oblique for finite size differences and horizontal when there is no size difference. Angle et al. [36] studied the orientation and terminal velocity of cylinders settling in quiescent water with both uniform and non-uniform distribution of mass. Their observations demonstrated that the cylinder with non-uniform mass distribution settles vertically at AR = 1, while it settles with a slightly oblique orientation at AR = 2 and 4. In the cases where the cylinders adopted oblique orientations, they exhibited horizontal displacement towards the initial location of the denser end of the particle along their trajectory.

Many models that relate drag coefficients and Reynolds number for non-spherical geometries falling in air or liquid are not accurate in predicting the terminal velocity or transport of single fibres. Additionally, the effect of curvature and bend in the geometry of individual cylindrical rods on their terminal velocity at low Reynolds numbers, representing the settling of microfibres in the air, is not yet extensively studied. To address this, we will conduct an experimental investigation to determine and compare the terminal velocities of cylindrical rods with four different geometries: straight, curved, V-shaped, and U-shaped. Our research aims to provide a deeper understanding of how various geometries affect the terminal velocity of microplastic fibres settling in the atmosphere. The following Section 2 describes the experimental methods, test specimens, and equipment. Results pertaining to the terminal velocity measurements are included in Section 3, followed by conclusions from this research in Section 4.

2. Materials and Methods

The Reynolds number range (based on the diameter of a volume-equivalent sphere) associated with the microfibres settling in the atmosphere was predicted using the microfibre dimensions reported in the literature [5, 37-40] and the

Henn model [25]. The calculations suggest that the Reynolds number is smaller than 5. Glycerin/water mixture with viscosities up to 1000 times as large as that of water enables us to use millimeter-scale metallic rods and makes it feasible to to track the 3D fall trajectory and individual orientation of these cylindrical rods within the atmospheric Reynolds number number range.

The straight, curved, V-shaped, and U-shaped cylindrical rods investigated in this research are all made of brass with a with a density of 8730±49 kg/m^3 and have diameters (D_C) of 0.50, 0.81, and 1.0 mm (with an uncertainty of ±0.05 mm) and aspect ratios (AR) varying from 10 to 120. The rods were cut with the mentioned aspect ratios with a tolerance of 0.1 mm. A schematic of the studied rods is shown in Figure 1. The radius of curvature (ROC) of the curved rods ranges from 19.90 mm to 36.40 mm, the bend angle (α) of the V-shaped rods varies between 45 and 135 degrees, and the length ratio of the middle arm (L_2) to the side arm (L_1) for the U-shaped rods is 1. The degree of curvature and bend for the curved and V-shaped rods respectively is denoted as C and defined as

$$C = 1 - \frac{L_P}{L_C}\ , \tag{1}$$

where L_P is the projected length of the curved and V-shaped rods (shown in Figure 1) and L_C is the total length of the rod. Table 1 shows the dimensions of the rod geometries used in this study.

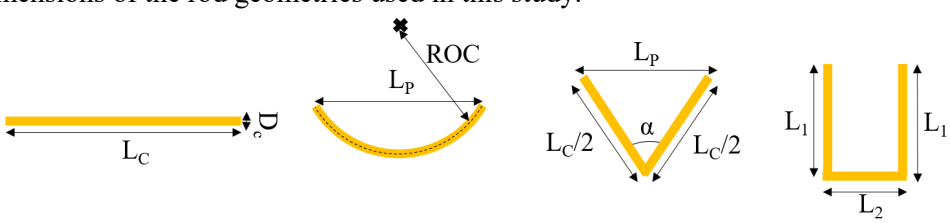

Figure 1: Schematic of the straight, curved, V-shaped, and U-shaped rods used in this research. L_C: total length of the rod, D_C: rod diameter, ROC: radius of curvature, α: bend angle, L_P: projected length, L_1: the length of the U-shaped side arm, and L_2: the length of the U-shaped middle arm.

Table 1: The rod geometries studied in this research (*Dc* is the rod diameter, *AR* is the rod aspect ratio, *ROC* is the radius of curvature for curved rods, and *α* is the bend angle for V-shaped rods)

Geometry	D_C (mm)	*AR*										*ROC* (mm)				*α* (degrees)				
		10	20	30	40	45	50	60	70	90	120	19.9	27.3	31.7	36.4	45	70	90	110	135
Straight	0.50	×	×	×				×		×	×									
	0.81	×	×	×	×		×	×	×	×										
	1.00	×	×	×		×	×													
Curved	0.50							×		×		×	×	×	×					
	1.00			×		×						×	×	×	×					
V-Shaped	0.50		×	×				×		×						×	×	×	×	×
U-Shaped	0.50			×	×		×	×		×										
	0.81			×	×		×	×		×										

Figure 2 shows the experimental setup. Two monochromatic cameras (Iron CXP 250) are positioned to face two perpendicular sides of the chamber, capturing the trajectory and orientation of cylindrical rods as they fall within the quiescent glycerin/water chamber. A third camera, situated underneath the tank, is utilized to observe the spinning motion of the falling rods around the vertical axis. The falling rod is illuminated by two 10-watt LED lights and acrylic diffuser plates placed behind the chamber. The chamber is filled with a mixture of 90% glycerine and 10% water. A Discovery HR-3 Hybrid Rheometer with a concentric cylinder geometry is used to measure the viscosity of this mixture with an uncertainty of 0.3%. The temperature of the glycerin/water mixture is monitored using a T-type thermocouple with an uncertainty of

±0.1 ºC which is permanently positioned inside the chamber. MATLAB is used to analyze the images from the cameras, and then a calibration algorithm is used to convert the pixel coordinates to real-life coordinates [41, 42]. The settling velocity of the rods is determined by dividing the displacement of the rod centroid between two consecutive images by the time interval between frames. The terminal velocity is defined as the average velocity during the last 10 cm of the rod descent inside the chamber. In order to confirm that the rod has reached its terminal velocity, it is checked that the settling velocity shows random variations of less than 1% compared to the average velocity over the last 10 cm of its trajectory as it approaches the bottom of the tank.

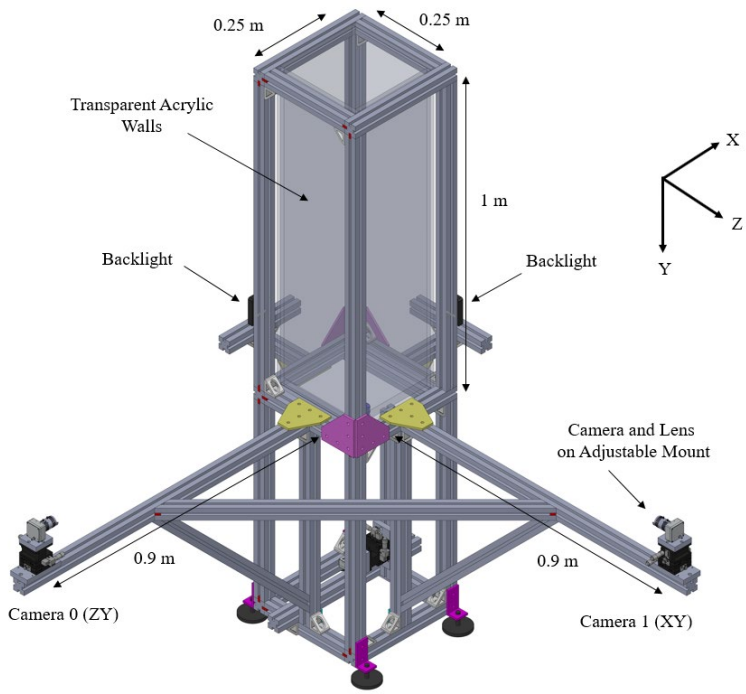

Figure 2: A schematic of the experimental setup including the quiescent glycerin chamber, cameras, and backlighting.

3. Results

The terminal velocities of the straight, curved, V-shaped, and U-shaped rods studied in this research are discussed in this section.

3.1. Straight Rods

The terminal velocities of the straight rods for the studied diameters and aspect ratios are plotted in Figure 3. This figure shows that as the diameter and aspect ratio of the rod increase, the rod terminal velocity increases. The rate of the change in the terminal velocity decreases with an increase in aspect ratio, leading to an asymptotic behaviour at high aspect ratios. This asymptotic trend also aligns with the findings from Jayaweera and Mason [43]. Furthermore, this figure compares the terminal velocity of the rod with $D_C = 0.5$ mm with the results of Song [22] and Henn [25] models. This comparison shows that Song model [22] fails to provide an accurate prediction for the terminal velocities of the rods within the ranges studied in this research since this model is developed for a wide range of particle geometries and consequently has lower accuracy for cylindrical particles. Henn model [25] aligns more closely with the experimental results obtained in this research. However, this model cannot still capture the asymptotic behaviour of the rod terminal velocity at high aspect ratios. The data points shown in Figure 3 are associated with a range of Reynolds numbers, which is calculated based on the diameter of the volume-equivalent sphere, between 0.07 and 1.75.

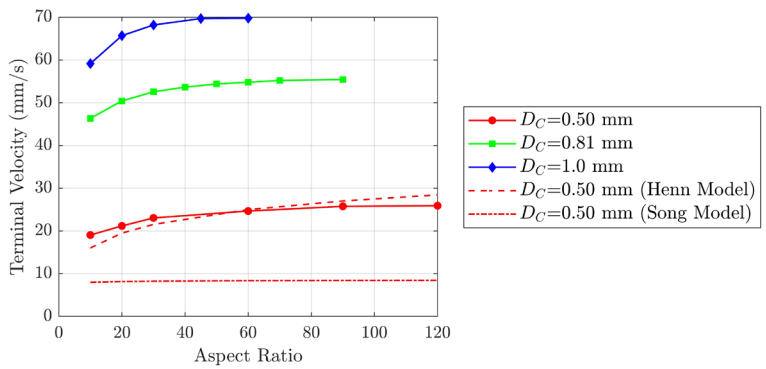

Figure 3: Terminal velocity of the straight rods for three rod diameters of 0.50, 0.81, and 1.0 mm at different aspect ratios. The dashed and dash-dotted lines represent the Henn [25] and Song [22] models respectively.

3.2. Curved Rods

Figure 4 illustrates the terminal velocities of the curved rods at different degrees of curvature ranging between 0.03 and 0.20 (refer to equation (1) and Figure 1) and compares them with those of the straight rods. It can be seen from this figure that the terminal velocity of a curved rod is always larger than that of a straight rod with the same diameter and aspect ratio. This can be attributed to the smaller projected area of the curved rods compared to the straight rods with the same dimensions. Furthermore, as the degree of curvature of the rod increases, or in other words, as the radius of curvature decreases, the terminal velocity increases. The terminal velocity of the curved rods is found to be up to 17% more than the terminal velocity of the straight rods based on the results in this study.

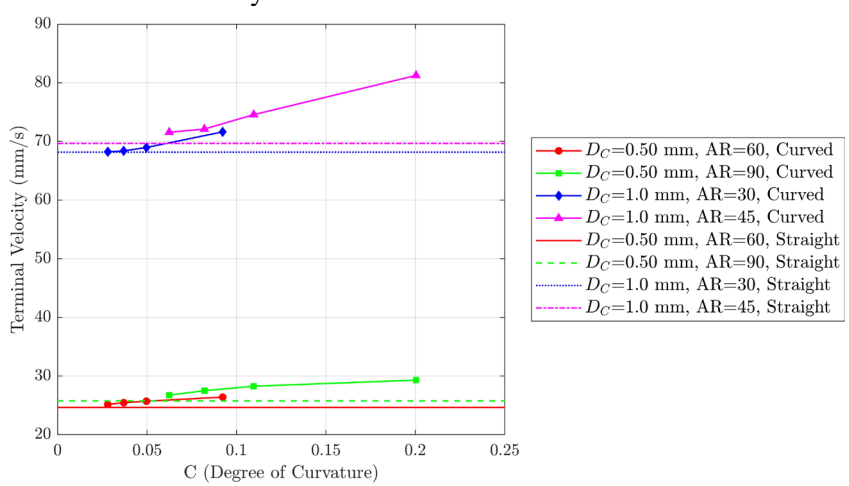

Figure 4: Terminal velocity of the curved rods at different degrees of curvature for two diameters of 0.50 and 1.0 mm and two aspect ratios of 60 and 90 as well as the straight rods with the same diameter and aspect ratio.

2.3. V-shaped Rods

Straight rods with the diameter of 0.50 mm are bent with the angles of 45, 70, 90, 110, and 135 degrees to make V-shaped rods with their degrees of bend ranging between 0.08 and 0.62. The terminal velocities of the V-shaped rods are plotted in Figure 5 at different degrees of bend. The results demonstrate that an increase in the degree of bend, corresponding to a decrease in the bend angle, results in a larger terminal velocity. The V-shaped rods always settle faster than the straight rods with the same diameter and aspect ratio. In addition to the smaller projected area of a V-shaped rod compared to a straight rod with the same dimensions, the V-shaped rod resembles two smaller rods connected to each other at an angle of

α. Each smaller rod has an inclined orientation, resulting in a higher settling velocity compared to a straight rod, which has a completely horizontal orientation. Moreover, the calculations show a maximum increase of 57% in the terminal velocity of the V-shaped rods relative to the straight rods within the ranges studied in this research.

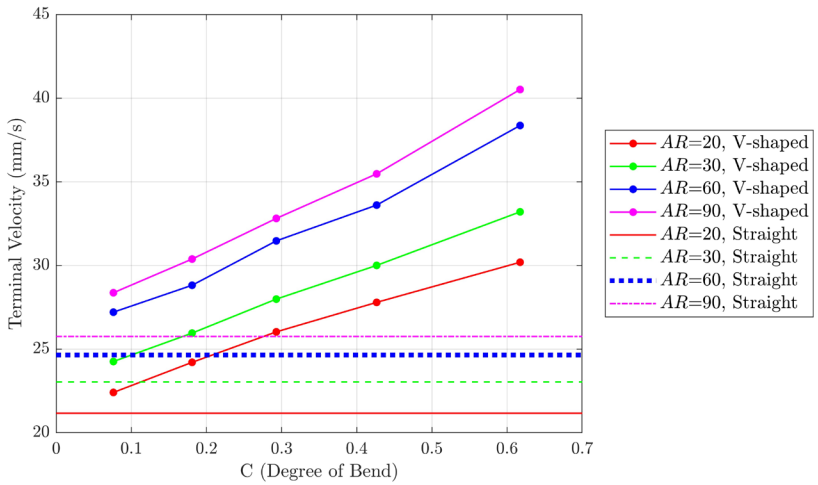

Figure 5: Terminal velocity of the V-shaped rods at different degrees of bend for the rod diameter of 0.50 mm and four aspect ratios of 20, 30, 60, and 90 as well as the straight rods with the same diameter and aspect ratio.

2.4. U-shaped Rods

Based on the observations in this research, the U-shaped rods adopt an oblique orientation during their fall, leading to a horizontal drift in their trajectory. In this study, the orientation of the U-shaped rods is defined by the angle between the U-shaped side arm and the horizontal direction, as shown in Figure 6. This angle is referred to as the "inclination angle", and is denoted by θ.

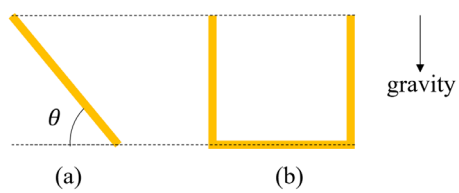

Figure 6: A (a) side and (b) front view of the U-shaped rod during its fall. The angle between the side arm and the horizontal direction, denoted by θ, is called the inclination angle and shows the orientation of the rod.

Figure 7 shows the variation of the U-shaped rod terminal velocity and inclination angle with the rod aspect ratio with all three arms equal ($L_1 = L_2$, L_1 and L_2 are represented in Figure 1). It can be seen from this figure that the terminal velocity of a U-shaped rod has a strong correlation with the inclination angle. For instance, for $D_C = 0.50$ mm, as the aspect ratio increases, the inclination angle changes from 90 degrees (vertical orientation) to 40 degrees (oblique orientation). This results in an increase in the terminal velocity from 33 to 38 mm/s and a decrease from 38 to 35 mm/s as the aspect ratio increases. However, the rod terminal velocity remains almost constant with the change in the aspect ratio for $D_C = 0.81$ mm since its inclination angle changes only from 37 to 25 degrees. The observed trends in the terminal velocity of the U-shaped rod as the aspect ratio increases can be explained by the interplay between the size and orientation of the rod. As the aspect ratio of the rod increases, the inclination angle decreases and the rod aligns more horizontally, which leads to a decrease in the terminal velocity. However, the side arms of the U-shaped rod increase in length with the increase in aspect ratio, which results in an increase in the terminal velocity. The mentioned counteracting factors cause the U-shaped rod to showcase either an initial increase and a subsequent decrease in the terminal velocity

(as observed for D_C = 0.50 mm) or an approximately constant value (as observed for D_C = 0.81 mm) as the aspect ratio increases. Furthermore, Figure 7 demonstrates that the terminal velocity of a U-shaped rod is always larger than a straight rod with the same diameter and aspect ratio due to the non-zero inclination of the U-shaped rods. The maximum difference difference between the U-shaped and the straight rod terminal velocity is determined to be 39% in this study.

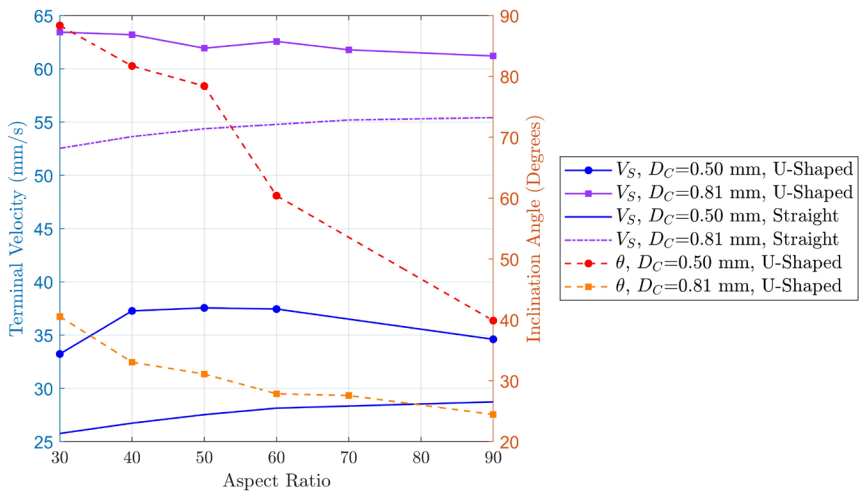

Figure 7: Variation of the U-shaped and straight rod terminal velocity as well as the U-shaped rod inclination angle (θ) with aspect ratio.

4. Conclusions

In this research, the atmospheric settling of microplastic fibres is experimentally replicated by performing drop tests with straight, curved, V-shaped, and U-shaped cylindrical rods all made of brass in a chamber filled with quiescent 90% glycerin/water mixture. The terminal velocity of the falling rods is determined by analyzing the images captured from two cameras facing the two perpendicular sides of the chamber. The results indicate that the terminal velocity of a straight rod increase with the rods diameter and aspect ratio, showcasing an asymptotic behavior towards a constant value at high aspect ratios, which is consistent with previous studies in the literature. The terminal velocity of the curved and the V-shaped rods increases with the degree of curvature and bend, which are associated with a decrease in the radius of curvature and bend angle for the curved and V-shaped rods respectively. The curved and V-shaped rods are found to settle faster than the straight rods with the same diameter and aspect ratio, with a maximum difference of 17% and 57% for the curved and V-shaped rods respectively in this study. The terminal velocity of a U-shaped rod is determined by the trade-off between the length of its arm and the rod orientation. An increase in the aspect ratio of a U-shaped rod results in a decrease in its inclination angle and an increase in the length of the rod arms. This leads to the terminal velocity of the rod either first increasing and then decreasing or remaining constant as the rod aspect ratio increases. The terminal velocity of the U-shaped rod is strongly correlated with the inclination angle and consistently greater than that of a straight rod with the same diameter and aspect ratio, with a maximum difference of 39% within the ranges studied in this research. According to the results in this research, V-shaped microfibres in the atmosphere exhibit higher vertical terminal velocity than U-shaped microfibres, U-shaped microfibre settling velocity exceeds curved microfibre settling velocity, and curved microfibre settling velocity exceeds that of straight microfibres, all with the same diameter and aspect ratio. Give this difference in settling velocity, we would expect curvature and bending to affect the horizontal transport distance of microplastic particles in the atmosphere, with the degree of bending leading to less horizontal transport relative to straight fibres.

Acknowledgements

This project is funded [in part] by the Northern Contaminants Program (CIRNAC, M-61) and the Government of Canada (ECCC, Grants and Contributions Award GCXE21S030).

References

[1] F. Petersen and J. A. Hubbart, "The occurrence and transport of microplastics: The state of the science," *Science of the Total Environment,* vol. 758, p. 143936, 2021.

[2] Y. Zhang, S. Kang, S. Allen, D. Allen, T. Gao, and M. Sillanpää, "Atmospheric microplastics: A review on current status and perspectives," *Earth-Science Reviews,* vol. 203, p. 103118, 2020.

[3] S. O'Brien, C. Rauert, F. Ribeiro, E. D. Okoffo, S. D. Burrows, J. W. O'Brien, X. Wang, S. L. Wright, and K. V. Thomas, "There's something in the air: A review of sources, prevalence and behaviour of microplastics in the atmosphere," *Science of The Total Environment,* vol. 874, p. 162193, 2023.

[4] S. Allen, D. Allen, F. Baladima, V. Phoenix, J. Thomas, G. Le Roux, and J. Sonke, "Evidence of free tropospheric and long-range transport of microplastic at Pic du Midi Observatory," *Nature communications,* vol. 12, no. 1, pp. 1-10, 2021.

[5] M. Bergmann, S. Mützel, S. Primpke, M. B. Tekman, J. Trachsel, and G. Gerdts, "White and wonderful? Microplastics prevail in snow from the Alps to the Arctic," *Science advances,* vol. 5, no. 8, p. eaax1157, 2019.

[6] S. L. Wright, J. Ulke, A. Font, K. L. A. Chan, and F. J. Kelly, "Atmospheric microplastic deposition in an urban environment and an evaluation of transport," *Environment international,* vol. 136, p. 105411, 2020.

[7] I. Napper, F. Parker-Jurd, S. Wright, and R. Thompson, "Examining the release of synthetic microfibres to the environment via two major pathways: Atmospheric deposition and treated wastewater effluent," *Science of The Total Environment,* vol. 857, p. 159317, 2023.

[8] J. C. Prata, "Airborne microplastics: consequences to human health?," *Environmental pollution,* vol. 234, pp. 115-126, 2018.

[9] K. Liu, X. Wang, T. Fang, P. Xu, L. Zhu, and D. Li, "Source and potential risk assessment of suspended atmospheric microplastics in Shanghai," *Science of the total environment,* vol. 675, pp. 462-471, 2019.

[10] S. Huang, X. Huang, R. Bi, Q. Guo, X. Yu, Q. Zeng, Z. Huang, T. Liu, H. Wu, and Y. Chen, "Detection and analysis of microplastics in human sputum," *Environmental Science & Technology,* vol. 56, no. 4, pp. 2476-2486, 2022.

[11] G. F. Chen, Qingyuan; Wang, Jun, "Mini-review of microplastics in the atmosphere and their risks to humans," *Science of the Total Environment,* vol. 703, 2020.

[12] P. Wu, S. Lin, G. Cao, J. Wu, H. Jin, C. Wang, M. H. Wong, Z. Yang, and Z. Cai, "Absorption, distribution, metabolism, excretion and toxicity of microplastics in the human body and health implications," *Journal of Hazardous Materials,* vol. 437, p. 129361, 2022.

[13] M. E. Çıtar Dazıroğlu and S. Bilici, "The hidden threat to food safety and human health: microplastics," *Environment, Development and Sustainability,* pp. 1-23, 2023.

[14] R. W. Obbard, S. Sadri, Y. Q. Wong, A. A. Khitun, I. Baker, and R. C. Thompson, "Global warming releases microplastic legacy frozen in Arctic Sea ice," *Earth's Future,* vol. 2, no. 6, pp. 315-320, 2014.

[15] F. Haque and C. Fan, "Fate of microplastics under the influence of climate change," *Iscience,* 2023.

[16] L. Cai, J. Wang, J. Peng, Z. Tan, Z. Zhan, X. Tan, and Q. Chen, "Characteristic of microplastics in the atmospheric fallout from Dongguan city, China: preliminary research and first evidence," *Environmental Science and Pollution Research,* vol. 24, no. 32, pp. 24928-24935, 2017.

[17] R. Dris, J. Gasperi, V. Rocher, M. Saad, N. Renault, and B. Tassin, "Microplastic contamination in an urban area: a case study in Greater Paris," *Environmental Chemistry,* vol. 12, no. 5, pp. 592-599, 2015.

[18] S. Allen, D. Allen, V. R. Phoenix, G. Le Roux, P. Durántez Jiménez, A. Simonneau, S. Binet, and D. Galop, "Atmospheric transport and deposition of microplastics in a remote mountain catchment," *Nature Geoscience,* vol. 12, no. 5, pp. 339-344, 2019.

[19] X. Long, T.-M. Fu, X. Yang, Y. Tang, Y. Zheng, L. Zhu, H. Shen, J. Ye, C. Wang, and T. Wang, "Efficient atmospheric transport of microplastics over Asia and adjacent oceans," *Environmental Science & Technology,* vol. 56, no. 10, pp. 6243-6252, 2022.

[20] E. E. Michaelides and Z. Feng, "Drag Coefficients of Non-Spherical and Irregularly Shaped Particles," *Journal of Fluids Engineering,* vol. 145, no. 6, p. 060801, 2023.

[21] G. H. Ganser, "A rational approach to drag prediction of spherical and nonspherical particles," *Powder technology,* vol. 77, no. 2, pp. 143-152, 1993.

[22] X. Song, Z. Xu, G. Li, Z. Pang, and Z. Zhu, "A new model for predicting drag coefficient and settling velocity of spherical and non-spherical particle in Newtonian fluid," *Powder Technology,* vol. 321, pp. 242-250, 2017.

[23] G. Bagheri and C. Bonadonna, "On the drag of freely falling non-spherical particles (vol 30, pg 526, 2016)," *Powder Technology,* vol. 349, pp. 108-108, 2019.

[24] J. Zhang and C. E. Choi, "Improved settling velocity for microplastic fibers: A new shape-dependent drag model," *Environmental science & technology,* vol. 56, no. 2, pp. 962-973, 2021.

[25] A. R. Henn, "Calculation of the stokes and aerodynamic equivalent diameters of a short reinforcing fiber," *Particle & particle systems characterization,* vol. 13, no. 4, pp. 249-253, 1996.

[26] A. Khalili and B. Liu, "Stokes' paradox: creeping flow past a two-dimensional cylinder in an infinite domain," *Journal of Fluid Mechanics,* vol. 817, pp. 374-387, 2017.

[27] B. Huner and R. Hussey, "Cylinder drag at low Reynolds number," *The Physics of Fluids,* vol. 20, no. 8, pp. 1211-1218, 1977.

[28] S. Sen, S. Mittal, and G. Biswas, "Steady separated flow past a circular cylinder at low Reynolds numbers," *Journal of Fluid Mechanics,* vol. 620, pp. 89-119, 2009.

[29] S. Dehghani, F. Moore, and R. Akhbarizadeh, "Microplastic pollution in deposited urban dust, Tehran metropolis, Iran," *Environmental Science and Pollution Research,* vol. 24, no. 25, pp. 20360-20371, 2017.

[30] S. Xiao, Y. Cui, J. Brahney, N. M. Mahowald, and Q. Li, "Long-distance atmospheric transport of microplastic fibres influenced by their shapes," *Nature Geoscience,* pp. 1-8, 2023.

[31] X. Rong, D. Qi, G. He, J. Zhu, and T. Scott, "Single curved fiber sedimentation under gravity," *Computers & Mathematics with Applications,* vol. 55, no. 7, pp. 1560-1567, 2008.

[32] X. Yang, Y. Wang, Y. Li, Y. Cao, Y. Zhou, and Y. Huang, "Experimental research on the settling property of slender fiber particles under the influence of multiple factors," *Powder Technology,* vol. 405, p. 117543, 2022.

[33] T. H. Nguyen, T.-C. Kieu-Le, F. H. Tang, and F. Maggi, "Controlling factors of microplastic fibre settling through a water column," *Science of The Total Environment,* p. 156011, 2022.

[34] B. Marchetti, V. Raspa, A. Lindner, O. Du Roure, L. Bergougnoux, E. Guazzelli, and C. Duprat, "Deformation of a flexible fiber settling in a quiescent viscous fluid," *Physical Review Fluids,* vol. 3, no. 10, p. 104102, 2018.

[35] A. Roy, R. J. Hamati, L. Tierney, D. L. Koch, and G. A. Voth, "Inertial torques and a symmetry breaking orientational transition in the sedimentation of slender fibres," *Journal of Fluid Mechanics,* vol. 875, pp. 576-596, 2019.

[36] B. R. Angle, M. J. Rau, and M. L. Byron, "Effect of mass distribution on falling cylindrical particles at intermediate Reynolds numbers," in *Fluids Engineering Division Summer Meeting*, 2019, vol. 59087: American Society of Mechanical Engineers, p. V005T05A065.

[37] M. Klein and E. K. Fischer, "Microplastic abundance in atmospheric deposition within the Metropolitan area of Hamburg, Germany," *Science of the Total Environment,* vol. 685, pp. 96-103, 2019.

[38] R. Dris, J. Gasperi, C. Mirande, C. Mandin, M. Guerrouache, V. Langlois, and B. Tassin, "A first overview of textile fibers, including microplastics, in indoor and outdoor environments," *Environmental pollution,* vol. 221, pp. 453-458, 2017.

[39] B. Roblin, M. Ryan, A. Vreugdenhil, and J. Aherne, "Ambient atmospheric deposition of anthropogenic microfibers and microplastics on the western periphery of Europe (Ireland)," *Environmental science & technology,* vol. 54, no. 18, pp. 11100-11108, 2020.

[40] S. Xiao, Y. Cui, J. Brahney, N. Mahowald, and Q. Li, "Long-distance atmospheric transport of microplastic fibers depends on their shapes," 2023.

[41] B. Wieneke, "Volume self-calibration for 3D particle image velocimetry," *Experiments in fluids,* vol. 45, no. 4, pp. 549-556, 2008.

[42] S. M. Soloff, R. J. Adrian, and Z.-C. Liu, "Distortion compensation for generalized stereoscopic particle image velocimetry," *Measurement science and technology,* vol. 8, no. 12, p. 1441, 1997.

[43] K. Jayaweera and B. Mason, "The behaviour of freely falling cylinders and cones in a viscous fluid," *Journal of Fluid Mechanics,* vol. 22, no. 4, pp. 709-720, 1965.